Hybridized magnon modes in the quenched skyrmion crystal

Rina Takagi, Markus Garst, Jan Sahliger, Christian H. Back, Yoshinori Tokura, and Shinichiro Seki

Phys. Rev. B **104**, 144410 — Published 12 October 2021

DOI: 10.1103/PhysRevB.104.144410

Hybridized magnon modes in the quenched skyrmion crystal

Rina Takagi[1,2,3,4], Markus Garst[5,6], Jan Sahliger[7],
Christian H. Back[7,8], Yoshinori Tokura[1,2,9], Shinichiro Seki[1,2,3,4]

[1] *RIKEN Center for Emergent Matter Science (CEMS), Wako 351-0198, Japan*
[2] *Department of Applied Physics, University of Tokyo, Tokyo 113-8656, Japan*
[3] *Institute of Engineering Innovation, University of Tokyo, Tokyo 113-0032, Japan*
[4] *PRESTO, Japan Science and Technology Agency (JST), Kawaguchi 332-0012, Japan*
[5] *Institut für Theoretische Festkörperphysik, Karlsruhe Institute of Technology, D-76131 Karlsruhe, Germany*
[6] *Institute for quantum materials and technology, Karlsruhe Institute of Technology, D-76021 Karlsruhe, Germany*
[7] *Physik-Department, Technische Universität München, D-85748 Garching, Germany*
[8] *Munich Center for Quantum Science and Technology (MCQST), D-80799 München, Germany and*
[9] *Tokyo College, University of Tokyo, Tokyo 113-8656, Japan*

Abstract

Magnetic skyrmions have attracted attention as particle-like swirling spin textures with nontrivial topology, and their self-assembled periodic order (i.e., skyrmion crystal (SkX)) is anticipated to host unique magnonic properties. In this study, we investigated magnetic resonance in the quenched SkX state, which is obtained by the rapid cooling of the high-temperature equilibrium SkX phase in the chiral magnetic insulator Cu_2OSeO_3. At low temperatures, novel sextupole and octupole excitation modes of skyrmions are identified, which are usually inactive for oscillating magnetic fields B^{ν} with GHz-range frequency ν but turn out to be detectable through the hybridization with the B^{ν}-active counter-clockwise and breathing modes, respectively. The observed magnetic excitation spectra are well reproduced by theoretical calculations, which demonstrates that the effective magnetic anisotropy enhanced at low temperatures is the key for the observed hybridization between the B^{ν}-active and B^{ν}-inactive modes.

Magnetic skyrmions, i.e. nanometric vortex-like swirling spin textures with topologically stable particle character, have attracted enormous attention[1–5]. Skyrmions can appear in form of either isolated particles or a periodically ordered state (i.e. skyrmion crystal (SkX) (Fig. 1(b))), and are usually stabilized in noncentrosymmetric magnets with Dzyaloshinskii-Moriya (DM) interaction in the presence of a static external magnetic field B_0. In metallic systems, skyrmions can be controlled by an electric current[6–9], and their nontrivial topology causes various intriguing transport phenomena such as a topological Hall effect[10,11]. Because of their electric controllability and small particle-like character, skyrmions are now intensively studied as promising components for the realization of high-density information storage[4,12,13].

Recently, skyrmions are also recognized as unique building blocks in the field of magnonics[14], and the detailed investigation of their resonant dynamics is highly demanded. Since the SkX state can be considered as a natural self-assembled magnonic crystal, the appearance of various nontrivial excitation modes is expected due to the backfolding of the spin wave dispersion. In previous magnetic resonance experiments, the equilibrium SkX state is reported to host three distinctive excitation modes, i.e., the clockwise (CW) and counter-clockwise (CCW) rotational modes that are excited by an oscillating magnetic field $B^\nu \perp B_0$, as well as the breathing mode active to $B^\nu \parallel B_0$ (Fig. 2(c))[15–19]. On the other hand, recent theoretical studies also predict the emergence of numerous B^ν-inactive excitation modes characterized by n-fold ($n = 2, 3, 4, ...$) shape deformations of skyrmions[14,20–22], while their experimental identification has hardly been achieved in the SkX state.

In this study, we report the clear experimental identification of the novel sextupole ($n = 3$) and octupole ($n = 4$) excitation modes in the quenched SkX state, which is obtained by the rapid cooling of the high-temperature equilibrium SkX phase for the chiral lattice insulator Cu_2OSeO_3. We found that B^ν-inactive sextupole and octupole modes hybridize with the B^ν-active CCW and breathing modes, respectively, and therefore become detectable by magnetic resonance experiments. Theoretical calculations demonstrate that magnetic anisotropies, which reduce the rotational symmetry of the effective theory, are at the origin of the observed hybridization between the B^ν-inactive and B^ν-active modes.

Our target material Cu_2OSeO_3 is characterized by a chiral cubic crystal structure with space group $P2_13$. This compound is known as the first insulating material to host skyrmion spin textures[23,24], and has been utilized as the prototypical system to study the magnon spectrum in the SkX state. Figure 1(a) indicates the B_0-T (temperature) magnetic phase diagram for Cu_2OSeO_3. The DM interaction stabilizes the helical magnetic order as the ground state for $B_0 = 0$, and the equilibrium SkX state, hosting the triangular lattice of skyrmions (Fig. 1(b)), appears in the narrow B_0-T region just below the magnetic ordering temperature $T_c \sim 58$ K. Recently, the appearance of another low-temperature skyrmion phase has also been reported for the high-B_0 region below 10 K (not shown)[22,25–27], where the formation of a long-range ordered skyrmion lattice structure is however hampered by very long equilibration times[22,25,26]. The latest magnetic resonance experiment in this low-temperature skyrmion phase suggests the potential observation of an octupole ($n = 4$) excitation mode[22], while the emergence of numerous extra modes (probably due to the disordered nature of skyrmion arrangement) prevented the clear mode assignment and quantitative analysis. Here, to realize a genuine SkX state at low temperature, we have prepared a micrometer-sized small crystal of Cu_2OSeO_3 (Fig. 1(c)), and rapidly cooled (~ 5 K/min) the high-temperature equilibrium SkX state following the path in the phase diagram indicated by the arrow in Fig. 1(a). Through this process, the SkX state can be kept down to the lowest temperature as a metastable state[28,29], since the reduction of the sample volume suppresses the nucleation probability of the competing helical/conical phase. Notably, it has been reported that the quenched SkX state in Cu_2OSeO_3 is long-range ordered[28], which would thus allow clear observation of the hybridization in the magnon spectrum. For such a quenched SkX state, we have performed the magnetic resonance experiments.

The bulk single crystals of Cu_2OSeO_3 were grown by the chemical vapor transport method. The device structure for the microwave absorption spectroscopy is shown in Figs. 1(c) and (d). A gold (Au) coplanar waveguide was prepared on the silicon substrate, and a plate-shaped Cu_2OSeO_3 single crystal with a thickness of 1 μm was mounted on the waveguide by using a focused ion beam (FIB) micro-fabrication system equipped with a scanning electron microscope (SEM). The sample was fixed by tungsten (W) bonding at one corner to avoid the tensile strain due to the mismatch of the thermal expansion coefficients at low temperature. By injecting an oscillating electric current I^ν with frequency ν into the waveguide, an oscillating magnetic field B^ν is generated and magnetic resonance is induced in the neighboring Cu_2OSeO_3 sample. The microwave absorption caused by magnetic resonance $\Delta S_{11}(\nu) = S_{11}(\nu) - S_{11}^{\mathrm{ref}}(\nu)$ was derived by subtraction of the common background $S_{11}^{\mathrm{ref}}(\nu)$ (taken at off-resonant condition for the target frequency range) from the raw reflection spectra $S_{11}(\nu)$, which were measured by a vector network analyzer[16,17,19]. The static magnetic field B_0 was applied perpendicular to the plane of the waveguide (i.e. parallel to the out-of-plane [001] direction of the sample). In this configuration, both modes active to $B^\nu \parallel B_0$ as well as $B^\nu \perp B_0$ can be excited. Note that the main excitation for the waveguide pattern in Fig. 1(c) lies at wavenumber $k = 0.25\mu\mathrm{m}^{-1}$, which is very close to $k = 0$ with respect to the Brillouin zone; therefore, magnetic resonance experiment here probes the response at practically zero momentum.

Figure 2(a) shows the magnetic field dependence of microwave absorption spectra measured in the metastable SkX state at 20 K after the field cooling through the path, indicated in Fig. 1(a). Here, mainly three distinctive magnetic resonance modes are identified. The high- and low-frequency modes with positive B_0 slopes correspond to the CW and CCW rotational modes, respectively, and the intermediate-frequency mode with negative B_0 slope represents the breathing mode. These behaviors are consistent with previous reports of the equilibrium SkX state[15–17], which confirms the realization of a pure SkX state at 20 K.

Interestingly, at this low temperature, we have discovered a clear splitting of the breathing mode at around $\nu \sim 4$ GHz and $B_0 \sim 120$ mT. The expanded view of the corresponding ν-B_0 region is shown in Fig. 3(a). The associated microwave absorption spectra, measured at various B_0-values, are indicated in Fig. 3(c). They can be fitted well by a single or two Lorentzian functions. In particular, two resonant excitation modes are identified for the B_0-value between 130 mT and 115 mT, whose peak frequencies are highlighted by triangular symbols. These two modes show anti-crossing-like behavior around 120 mT, while one other mode crossing the breathing mode loses the spectral intensity rapidly as departing from the crossing point.

To understand the microscopic origin of such an anomaly in the breathing mode, we have theoretically evaluated the magnetic excitation spectra in the SkX state. Here, we consider the density $\mathcal{F} = \mathcal{F}_0 + \mathcal{F}_{\mathrm{dip}} + \mathcal{F}_{\mathrm{cub}}$ of the magnetic energy functional in the continuum approximation, with its first term given by

$$\mathcal{F}_0 = \frac{J}{2}(\nabla \mathbf{m})^2 + D\mathbf{m} \cdot (\nabla \times \mathbf{m}) - M_s \mathbf{B}_0 \cdot \mathbf{m}. \tag{1}$$

J, D, and M_s are the exchange interaction, DM interaction and saturation magnetization, respectively. $\mathbf{B_0} = \mu_\mathbf{0}\mathbf{H_0}$ where μ_0 is the magnetic constant and $\mathbf{H_0}$ is the externally applied magnetic field, and $\mathbf{m}(\mathbf{r})$ is the unit vector pointing along the direction of the local magnetic moment. $\mathcal{F}_{\rm dip}$ and $\mathcal{F}_{\rm cub}$ represent the dipolar interaction and the cubic magnetic anisotropy. $\mathcal{F}_0+\mathcal{F}_{\rm dip}$ is symmetric with respect to a combined continuous rotation in real and spin spaces around the magnetic field axis. This rotational symmetry is explicitly broken by $\mathcal{F}_{\rm cub}$ which induces a hybridization between modes as demonstrated below. In the following, we restrict ourselves to magnetocrystalline anisotropies represented by $\mathcal{F}_{\rm cub} = -K(m_x^4 + m_y^4 + m_z^4)$, but similar results can be obtained for exchange anisotropies. For the present calculation, we employed the J, D, and M_s values specified for Cu_2OSeO_3 in Ref.[19] and a modest amplitude of anisotropy $K = 0.1D^2/J$. The demagnetization factor is deduced from the sample shape, and B_0 is applied along the z-axis. Following the theoretical approach of Refs.[17,19], the theoretically expected B_0-dependence of resonance parameters in the SkX state are calculated as shown in Fig. 2(b). Here, the size of each colored data point denotes the excitation amplitude for B^ν, and the calculated frequencies of CCW, CW, and breathing modes are quantitatively in good agreement with the experimental result. Importantly, the hybridization between the B^ν-active breathing mode and another B^ν-inactive excitation mode is clearly identified at $\nu \sim 4$ GHz and $B_0 \sim 120$ mT, which well reproduces the experimentally observed anomaly in the excitation spectra for the breathing mode. To understand the character of the latter B^ν-inactive skyrmion excitation mode, the corresponding time development of the $m_z(\mathbf{r})$ distribution is indicated in the middle column of Fig. 2(c). This mode induces the four-fold deformation of the skyrmion spin texture, and its pattern shows a continuous rotation as a function of time. Such an octupole skyrmion excitation mode is usually inactive for B^ν, due to the lack of a macroscopic magnetization oscillation[21]. By hybridizing with another B^ν-active mode, however, this B^ν-inactive excitation mode becomes detectable by magnetic resonance measurements.

Notably, the present calculation also predicts the hybridization between the B^ν-active CCW mode and the B^ν-inactive sextupole mode at $\nu \sim 2$ GHz and $B_0 \sim 130$ mT, where the sextupole mode is characterized by the three-fold deformation of the skyrmion spin texture as shown in the leftmost column of Fig. 2(c). Such a hybridization behavior is indeed observed in the experiments, and the expanded view of the corresponding ν-B_0 region is shown in Figs. 3(b) and (d). The associated microwave absorption spectra can be well fitted by a single or two Lorentian functions, and the two-peak structure due to the hybridization can be identified at $B_0 = 125$ and 130 mT. Here, we defined the hybridization gap Δ as the minimum difference of the two peak frequencies as shown in Fig. 4(a). The experimentally deduced $\Delta \sim 130$ MHz for the CCW/sextupole modes is much smaller than $\Delta \sim 370$ MHz for the breathing/octupole modes, which is also consistent with the theoretical prediction in Fig. 2(b).

Next, we investigated the temperature dependence of the hybridization behavior between the breathing and octupole modes as shown in Figs. 4(c)-(h). As the temperature increases, the hybridization gradually becomes obscure. Figure 4(a) shows the microwave absorption spectra at the B_0 value, giving the hybridization gap Δ at each temperature. The peak frequencies are determined from the spectral fitting with a double Lorentzian function (solid lines in Fig. 4(a)). With increasing temperature, the frequencies of two peaks get closer and finally merge into a single peak above 40 K. Figure 4(b) indicates the temperature dependence of the observed hybridization gap Δ, which demonstrates the clear enhancement of Δ at lower temperatures.

To understand the microscopic origin of the observed hybridization behavior and its temperature dependence, resonance parameters theoretically calculated for various K values in units of D^2/J are summarized in Fig. 5. We found that the hybridization for the breathing/octupole modes and the CCW/sextupole modes is absent for $K = 0$, while the size of the hybridization gap Δ gradually increases as a function of K. According to previous reports for Cu_2OSeO_3, the cubic magnetocrystalline anisotropy K monotonously increases with decreasing temperature below 40 K[26], which is consistent with the observed enhancement of Δ below 40 K. Using the reported K-value in Ref.[26], we theoretically calculated the hybridization gap Δ as a function of temperature, as shown in Fig. 4(b). This provides a parameter-free prediction for $\Delta(T)$ that is, however, smaller than the experimentally observed one by a factor of 2-3. Note that besides K there are additional contributions that also break the rotational symmetry and are of the same fourth order in spin-orbit coupling. In particular, exchange anisotropies will also result in a hybridization gap. In principle, a systematic treatment of all anisotropies is required in order to account quantitatively for the temperature dependence of Δ. However, such a treatment involves many parameters that cannot be uniquely determined by the experimentally accessible $\Delta(T)$ so that we refrain from such an analysis. Nevertheless, we can conclude from the above results that the cubic magnetic anisotropy is the main source of the observed hybridization, while for a consistent quantitative treatment of both thermodynamics[26] and the excitation dynamics both magnetocrystalline and exchange anisotropies need to be taken into account.

According to recent theoretical studies[14,20,21], B^{ν}-inactive n-fold shape-deformation modes are expected not only for the presently observed $n = 3$ (sextupole mode) and $n = 4$ (octupole mode) but also for general integer n-values, where the eigenfrequencies increase for larger n. Our results suggest that the other n-fold deformation modes of skyrmions may be also detectable through a similar hybridization approach by tuning the material parameters. Notably, these n-fold deformation modes are predicted to possess a nontrivially flat magnon dispersion within the two-dimensional SkX plane. This implies an anisotropic channeling effect for spin waves, where the magnons are localized along the SkX-plane direction and only propagate along the skyrmion string direction. In addition, some excitation modes in the SkX state are also predicted to host non-zero topological Chern numbers[14,20,21]. It would be interesting to investigate the Berry curvature and associated Chern number for the hybridized magnon modes, which is related to various intriguing phenomena such as a topological magnon Hall effect and magnon edge states.

In summary, by performing magnetic resonance experiments in the quenched SkX state, we have identified novel sextupole and octuple excitation modes of skyrmions. These modes are usually B^{ν}-inactive, but turned out to be detectable through the hybridization with B^{ν}-active CCW and breathing excitation modes, respectively. Compared to the artificial magnonic crystal, the self-assembled SkX state is characterized by a unique magnon spectrum with quantum numbers reflecting the degrees of freedom of a topologically protected particle-like spin texture. Since the associated excitation modes are predicted to host various exotic properties (such as flat magnon dispersion and/or nontrivial topological Chern number[14,20,21]), further investigation of the propagation dynamics of such hybridized magnon modes in the SkX state, which would be possible by propagating spin-wave spectroscopy[30,31] or Brillouin light scattering[32–34], is an attractive field of future research.

ACKNOWLEDGEMENTS

The authors thank M. Mochizuki for enlightening discussions. This work was partly supported by Grants-In-Aid for Scientific Research (Grants No. 18H03685, 20H00349, 21H04440, 21H04990, 21K18595, and 21K13876) from JSPS, PRESTO (Grant No. JPMJPR18L5 and JPMJPR20B4) and CREST (Grant No. JPMJCR1874) from JST, Asahi Glass Foundation and Murata Science Foundation. M.G. acknowledges financial support from DFG CRC 1143 (Project No. 247310070) and DFG Project No. 270344603 and 324327023. C.H.B. acknowledges funding from DFG via SPP2137 (Project No. 360506545, 403194850) and the excellence cluster MCQST under Germany's Excellence Strategy EXC-2111 (Project No. 390814868).

---

[1] S. Mühlbauer, B. Binz, F. Jonietz, C. Pfleiderer, A. Rosch, A. Neubauer, R. Georgii, and P. Böni, Science **323**, 915 (2009).

[2] X. Z. Yu, Y. Onose, N. Kanazawa, J. H. Park, J. H. Han, Y. Matsui, N. Nagaosa, Y. Tokura, Nature **465**, 901 (2010).

[3] U. K. Rößler, A. N. Bogdanov, and C. Pfleiderer, Nature **442**, 797 (2006).

[4] A. Fert, N. Reyren, V. Cros, Nature Rev. Mater, **2**, 17031 (2017).

[5] N. Nagaosa, Y. Tokura, Nature Nanotech. **8**, 899 (2013).

[6] F. Jonietz, S. Mühlbauer, C. Pfleiderer, A. Neubauer, W. Münzer, A. Bauer, T. Adams, R. Georgii, P. Böni, R. A. Duine, K. Everschor, M. Garst, and A. Rosch, Science **330**, 1648 (2010).

[7] X. Z. Yu, N. Kanazawa, W. Z. Zhang, T. Nagai, T. Hara, K. Kimoto, Y. Matsui, Y. Onose, and Y. Tokura, Nature Commun. **3**, 988 (2012).

[8] W. Jiang, P. Upadhyaya, W. Zhang, G. Yu, M. B. Jungfleisch, F. Y. Fradin, J. E. Pearson, Y. Tserkovnyak, K. L. Wang, O. Heinonen, S. G. E. te Velthuis, A. Hoffmann, Science **349**, 283 (2015).

[9] S. Woo, K. Litzius, B. Krüger, M.-Y. Im, L. Caretta, K. Richter, M. Mann, A. Krone, R. M. Reeve, M. Weigand, P. Agrawal, I. Lemesh, M.-A. Mawass, P. Fischer, M. Kläui, and G. S. D. Beach, Nature Mater. **15**, 501 (2016).

[10] A. Neubauer, C. Pfleiderer, B. Binz, A. Rosch, R. Ritz, P. G. Niklowitz, and P. Böni, Phys. Rev. Lett. **102**, 186602 (2009).

[11] T. Schulz, R. Ritz, A. Bauer, M. Halder, M. Wagner, C. Franz, C. Pfleiderer, K. Everschor, M. Garst, and A. Rosch, Nature Phys. **8**, 301 (2012).

[12] X. Zhang, M. Ezawa, and Y. Zhou, Sci. Rep. **5**, 9400 (2015).

[13] K. M. Song, J.-S. Jeong, B. Pan, X. Zhang, J. Xia, S. Cha, T.-E. Park, K. Kim, S. Finizio, J. Raabe, J. Chang, Y. Zhou, W. Zhao, W. Kang, H. Ju, and S. Woo, Nature Electronics **3**, 148 (2020).

[14] M. Garst, J. Waizner, D. Grundler, J. Phys. D: Appl. Phys. **50**, 293002 (2017).

[15] M. Mochizuki, Phys. Rev. Lett. **108**, 017601 (2012).

[16] Y. Onose, Y. Okamura, S. Seki, S. Ishiwata, Y. Tokura, Phys. Rev. Lett. **109**, 037603 (2012).

[17] T. Schwarze, J. Waizner, M. Garst, A. Bauer, I. Stasinopoulos, H. Berger, C. Pfleiderer, D. Grundler, Nature Mater. **14**, 478 (2015).

[18] O. Petrova and O. Tchernyshyov, Phys. Rev. B **84**, 214433 (2011).

[19] S. Seki, M. Garst, J. Waizner, R. Takagi, N. D. Khanh, Y. Okamura, K. Kondou, F. Kagawa, Y. Otani, and Y. Tokura, Nature Comm. **11**, 256 (2020).

[20] A. Roldán-Molina, A. S. Nunez, and J. Fernández.-Rossier, New J. Phys. **18**, 045015 (2016).

[21] S. A. Díaz, T. Hirosawa, J. Klinovaja, and D. Loss, Phys. Rev. Res. **2**, 013231 (2020).

[22] A. Aqeel, J. Sahliger, T. Taniguchi, S. Mandl, D. Mettus, H. Berger, A. Bauer, M. Garst, C. Pfleiderer, C.H. Back, Phys. Rev. Lett. **126**, 017202 (2021).

[23] S. Seki, X. Z. Yu, S. Ishiwata, Y. Tokura, Science **336**, 198 (2012).

[24] T. Adams, A. Chacon, M. Wagner, A. Bauer, G. Brandl, B. Pedersen, H. Berger, P. Lemmens, C. Pfleiderer, Phys. Rev. Lett. **108**, 237204 (2012).

[25] A. Chacon, L. Heinen, M. Halder, A. Bauer, W. Simeth, S. Mühlbauer, H. Berger, M. Garst, A. Rosch, and C. Pfleiderer, Nature Phys. **14**, 936 (2018).

[26] M. Halder, A. Chacon, A. Bauer, W. Simeth, S. Mühlbauer, H. Berger, L. Heinen, M. Garst, A. Rosch, C. Pfleiderer, Phys. Rev. B **98**, 144429 (2018).

[27] L. J. Bannenberg, H. Wilhelm, R. Cubitt, A. Labh, M. P. Schmidt, E. L.-Berna, C. Pappas, M. Mostovoy, and A. O. Leonov, npj Quantum Mater. **4**, 11 (2019).

[28] R. Takagi, Y. Yamasaki, T. Yokouchi, V. Ukleev, Y. Yokoyama, H. Nakao, T. Arima, Y. Tokura, and S. Seki, Nature Commun. **11**, 5685 (2020).

[29] H. Oike, A. Kikkawa, N. Kanazawa, Y. Taguchi, M. Kawasaki, Y. Tokura, and F. Kagawa, Nature Phys. **12**, 62 (2016).

[30] V. Vlaminck and M. Bailleul, Science **322**, 410 (2008).

[31] V. Vlaminck and M. Bailleul, Phys. Rev. B **81**, 014425 (2010).

[32] K. Di, V. L. Zhang, H. S. Lim, S. C. Ng, M. H. Kuok, J. Yu, J. Yoon, X. Qiu, and H. Yang, Phys. Rev. Lett. **114**, 047201 (2015).

[33] J. Cho, N.-H. Kim, S. Lee, J.-S. Kim, R. Lavrijsen, A. Solignac, Y. Yin, D.-S. Han, N. J. J. van Hoof, H. J. M. Swagten, B. Koopmans, and C.-Y. You, Nat. Commun. **6**, 7635 (2015).

[34] N. Ogawa, L. Köhler, M. Garst, S. Toyoda, S. Seki, and Y. Tokura, Proc. Natl. Acad. Sci. USA **118**, e2022927118 (2021).

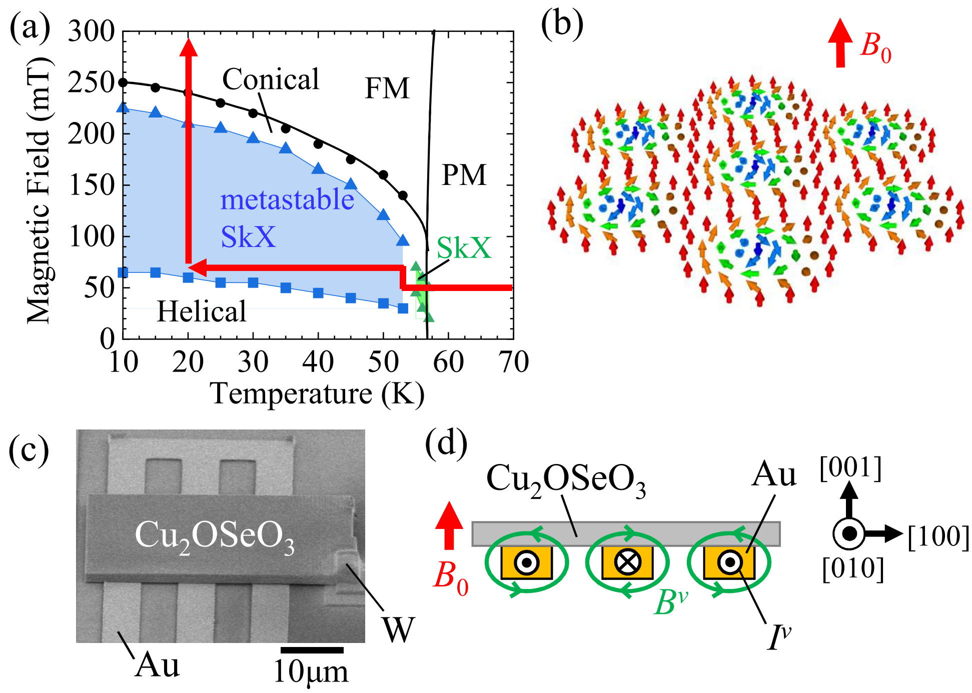

FIG. 1. (a) Magnetic field (B_0)-temperature (T) phase diagram for the field-cooling path shown by the arrows, determined by microwave absorption spectroscopy for Cu_2OSeO_3 with $B_0 \parallel [001]$. (b) Schematic illustration of a skyrmion crystal (SkX) spin texture. (c) SEM image of the device structure used for the microwave absorption spectroscopy. (d) Schematic side view of the device structure. By injecting an oscillating electric current I^ν of gigahertz frequency [black arrows pointing along the out-of-plane direction] into the Au coplanar waveguide, an oscillating magnetic field B^ν is generated and magnetic resonance is excited.

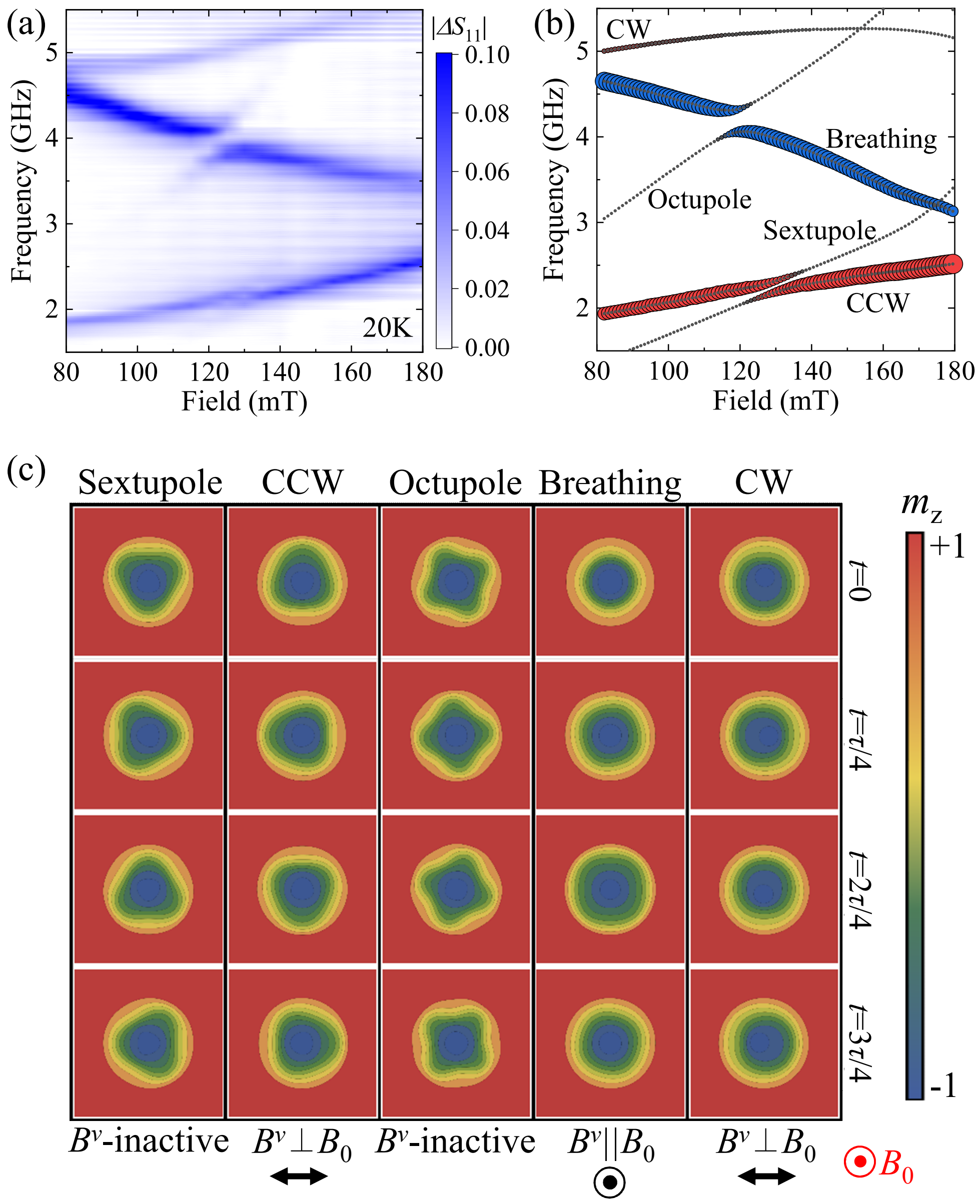

FIG. 2. (a) Magnetic field dependence of microwave absorption spectra in the SkX state for $B_0 \parallel [001]$ at 20 K. The background color represents the microwave absorption intensity $|\Delta S_{11}(\nu)|$. (b) Theoretically calculated magnetic excitation spectra as a function of $B_0 \parallel [001]$, with the cubic anisotropy parameter $K = 0.1D^2/J$ (see main text). The size of each colored point represents the excitation amplitude for B^ν. (c) Time(t)-development of the spatial distribution of $m_z(\mathbf{r})$ (the out-of-plane component of local magnetization) calculated for various excitation modes in the SkX state. τ represents the oscillation period. The polarization direction of B^ν to excite each resonance mode is also indicated at the bottom.

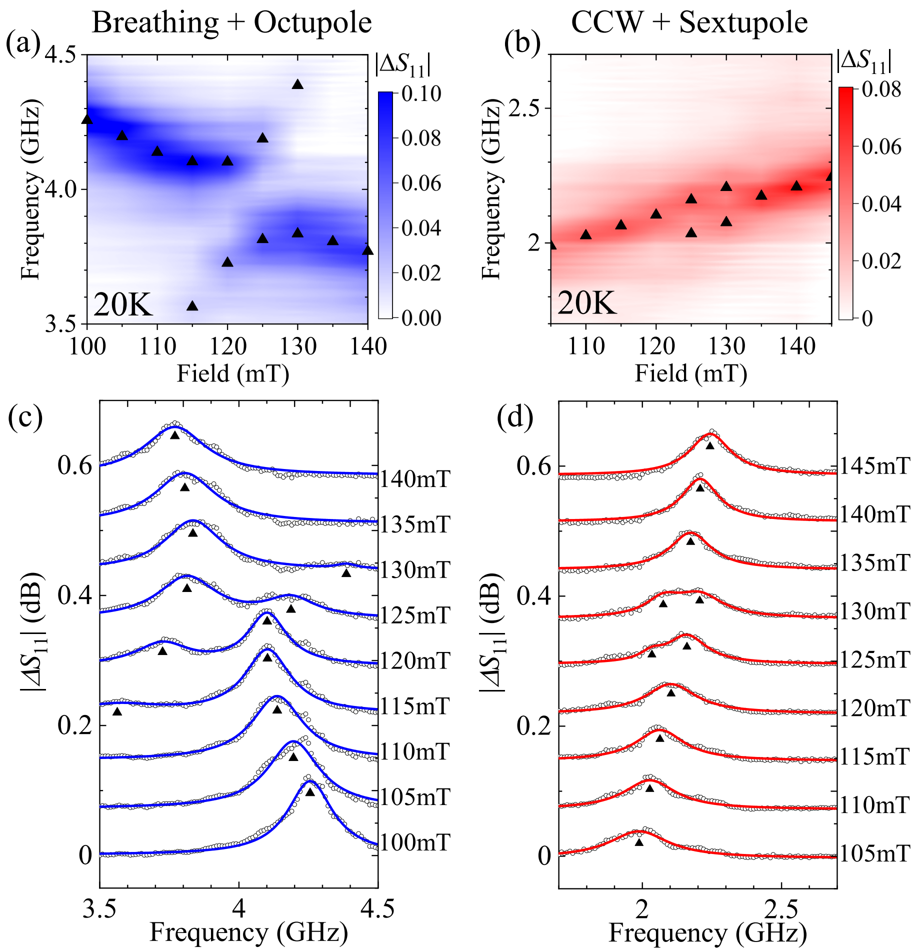

FIG. 3. (a),(b) The expanded view of Fig. 2(a) for the B_0-ν region representing the hybridization for (a) breathing/octupole modes and (b) CCW/sextupole modes at 20 K. (c),(d) Microwave absorption spectra corresponding to (a) and (b). The peak frequencies (triangles) are extracted from the spectral fitting with Lorentz function. The fitting curves are drawn by solid lines.

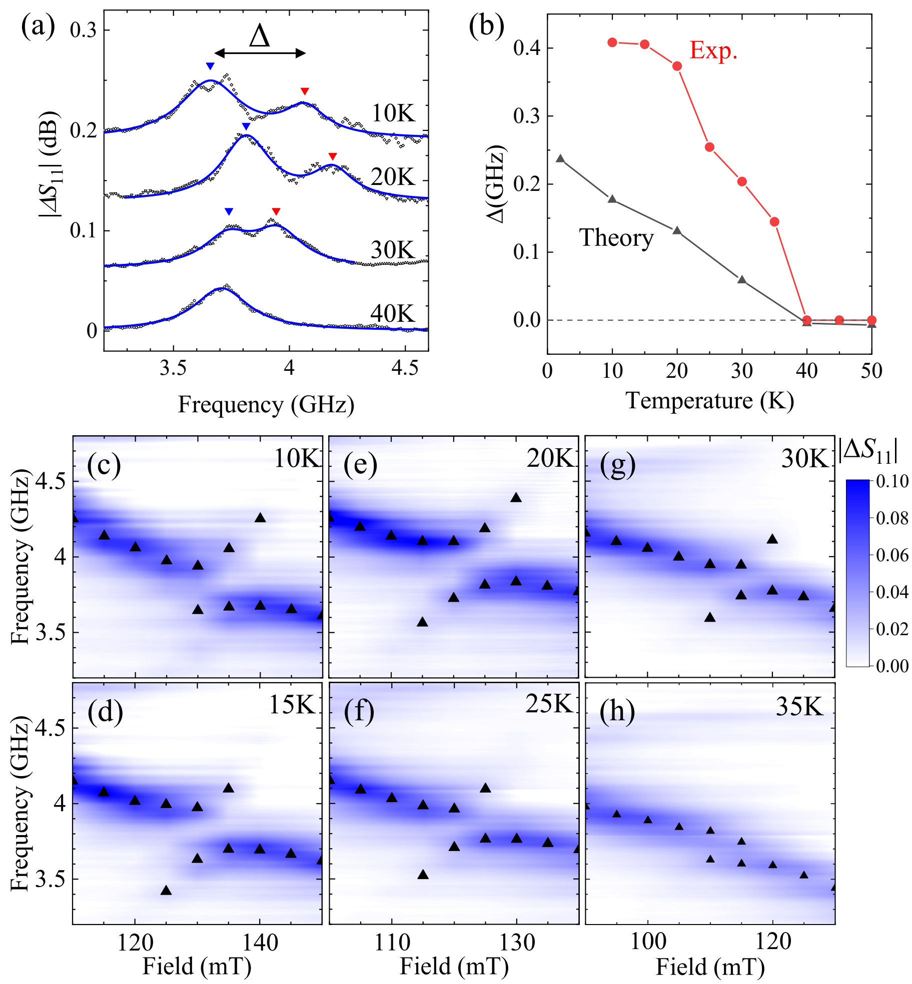

FIG. 4. (a) Microwave absorption spectra for B_0 giving the minimum value of the frequency difference between two peaks at each temperature. Solid lines are the results of the fitting with double Lorentz function. (b) Temperature dependence of the hybridization gap Δ for the breathing/octupole modes. (c)-(h) The hybridization of breathing/octupole modes at (c) 10 K, (d) 15 K, (e) 20 K, (f) 25 K, (g) 30 K, and (h) 35 K. Peak frequencies determined from the spectral fitting are depicted by triangles.

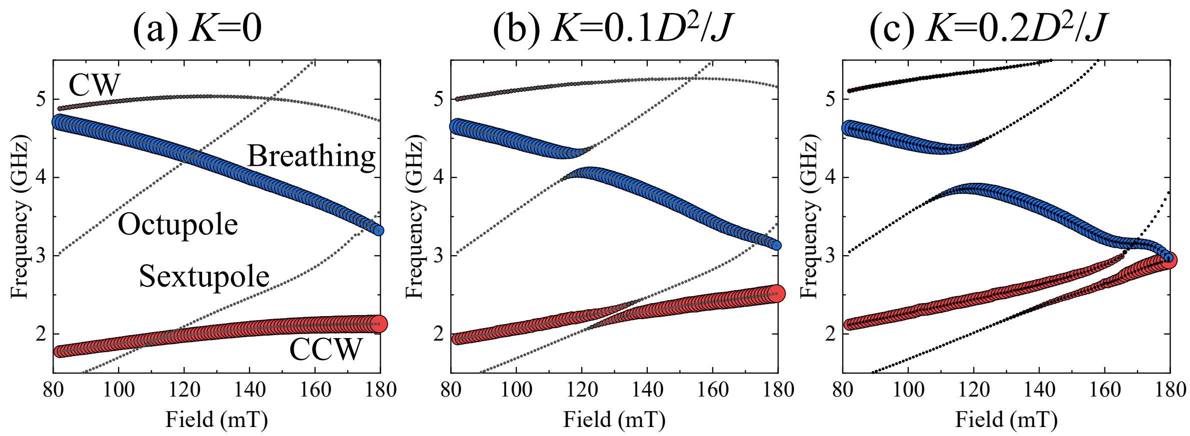

FIG. 5. Theoretically calculated magnetic excitation spectra as a function of $B_0 \parallel [001]$, with the cubic anisotropy parameter (a)$K = 0$, (b)$K = 0.1D^2/J$ and (c)$K = 0.2D^2/J$. The size of each data point represents the excitation amplitude for B^ν.